Title
STUDY OF 12C INTERACTIONS AT HISS



Author
Crawford, H.J.

Publication Date
1982-12-01

# Lawrence Berkeley Laboratory

UNIVERSITY OF CALIFORNIA



Presented at the Symposium on Detectors in Heavy Ion Physics, Hahn-Meitner Institute für Kernforschung, Berlin, West Germany, October 6-8, 1982

STUDY OF $^{12}C$ INTERACTIONS AT HISS

H.J. Crawford

December 1982



NUCLEAR SCIENCE DIVISION



Prepared for the U.S. Department of Energy under Contract DE-AC03-76SF00098

LBL-15447

# Study of $^{12}C$ Interactions at HISS

H.J. Crawford

HISS Group

Nuclear Science Division
Lawrence Berkeley Laboratory
Space Sciences Laboratory
University of California
Berkeley, CA 94720

Presented at The Symposium on Detectors
in Heavy Ion Physics, Hahn-Meitner
Institute für Kernforschung, Berlin
6-8 October 1982

This work was supported by the Director, Office of Energy Research, Division of Nuclear Physics of the Office of High Energy and Nuclear Physics of the U.S. Department of Energy under Contract DE-AC03-76SF00098 and National Aeronautics and Space Administration grant number NGR 03-003-513.

# STUDY OF 12C INTERACTIONS AT HISS

H.J. Crawford
HISS Group
Lawrence Berkeley Laboratory,
Space Sciences Laboratory,
University of California
Berkeley, California 94720

Single particle inclusive measurements in high energy nuclear physics have provided the foundation for a number of models of interacting nuclear fluids. Such measurements yield information on the endpoints of the evolution of highly excited nuclear systems. However, they suffer from the fact that observed particles can be formed in a large number of very different evolutionary paths. To learn more about how interactions proceed we have performed a series of experiments in which all fast nuclear fragments are analysed for each individual interaction. These experiments were performed at the LBL Bevalac HISS (Heavy Ion Spectrometer System) facility where we studied the interaction of 1 GeV/nuc 12C nuclei with targets of C, CH2, Cu, and U. In this paper we describe HISS and present some preliminary results of the experiment.

We first review some of the results of single particle inclusive measurements to illustrate the motivation for a facility such as HISS. These are summarized in fig. 1. Such properties suggest a schematic representation for relativistic heavy ion reactions such as shown in fig. 2. A question relevant to all three diagrams concerns the relation of the energy and momentum transferred at the vertex. It is possible that the vertex is complex, such as in a nuclear cascade, or single, such as in electromagnetic excitation of a giant dipole resonance. To measure this energy-momentum transfer we utilize the kinematic focussing property to investigate final states of the incident 12C nucleons. Theoretical predictions of the energy transfer spectrum from three different models are shown in fig. 3.

The HISS facility was constructed to allow particle identification (charge Z, mass M, and vector momentum P) for many particles from the same interaction. The facility consists of:

1. Large superconducting dipole;
2. Multi CPU computer system;
3. Trajectory measuring devices-Drift chambers;
4. Velocity measuring devices-Time-of-flight (TOF) array;
5. Charge measuring devices-Scintillators and MUSIC.

The floor layout of HISS at the Bevalac showing the dipole, cave area, electronics house, and VAX house is given in fig. 4. I would like to thank the many people whose names are shown in fig. 5 for making the HISS facility work.

The first five experiments accepted for running at HISS are summarized in fig. 6. These range in experimental complexity from single particle inclusive spectra to full event reconstruction. The HISS facility is equipped with a set of facility detectors described below and shown in fig. 7. It is often the case that a measurement will require additional detector systems. In fig. 8 we show the set up for the high Pperp experiment which has, in addition to the facility detectors, a set of MWPC and scintillators that operate in the field region of the dipole that were constructed by the INS group.

The heart of this HISS facility is a large (1 m gap, 2 m poletips), superconducting dipole (30kG field), capable of rotating through 360 degrees. We measure rigidity by determining particle trajectories through this field. The field is surface mapped (1cm grid) to an accuracy of 1 gauss. The surface map is converted to a volume map using LaPlace's equation in a VAX computer. A large number of sample trajectories are then sent through the volume and numerically integrated to return a set of Chebychev coefficients which give the vector momentum, rigidity, and pathlength from a set of input x, y, and z coordinates.

A multi CPU computer system is used at HISS to control the dipole, monitor the beam line during experiments, and gather and analyse data. The HISS computer system is shown in fig. 9. The basic data flow is from detectors through CAMAC into a micro-programmable branch driver (MBD) and then into a front-end acquisition CPU (11/45). There the data is spooled onto tape and onto an intermediate disk which has a port connection to the VAX so that complex on-line analyis can be performed (e.g. event reconstruction).

Particle identification at HISS is accomplished through measurements of rigidity, R (= momentum/charge), charge, Z, and velocity, $\beta$. We describe below the performance of the prototype Phase I detectors shown in fig. 6 and discuss some of the parameters of our upgraded Phase II array.

We use drift chambers upstream of the target to determine the incident beam trajectory and downstream to determine the trajectories of all fast charged fragments produced in the forward 5 degree cone. A schematic diagram of such a drift chamber is shown in fig. 10. Note that there are two vertical (or "S" plane) wires, two "T" plane (+60 degrees), and two "U" plane (-60 degrees) wires to remove the left-right ambiguity of a single wire measurement.

These chambers are designed to give locations for all charged fragments. Since the chambers must locate protons as well as heavy ions they must be sensitive to high energy delta rays as well. The track of a heavy ion must be determined in the presence of a large halo of high energy delta rays. To determine the location of the core ionization in a heavy ion track we use a dynamically set threshold on the timing discriminator for each wire as shown in fig. 11. This timing pulse is sent as a stop signal to a channel of LeCroy 4290 system TDC. The analog fraction of the signal is sent to a LeCroy 2880 system ADC for all of the "S" plane wires.

Each of the large drift chambers has six planes so that a good fragment track has 12 TDC values to be used to determine two x, y locations. To calibrate the system the time to distance function must be determined for each TDC-wire combination. The nonlinear time to distance function for a sample cell is seen in the scatter plot of TDC1 and TDC2 from the "S" plane of DC1. The width of the sum of the linearized TDC signals from such a pair gives us our single cell spatial resolution, shown in fig. 12 to be a FWHM of 200µ. This leads to a resolution for beam particles of dP/P = 0.001.

The time-of-flight (TOF) scintillator array is designed to measure the charge and flight time for fragments of charge 1 to 6. Each scintillator slat is 2.5 cm thick, 10 cm wide, and either 200 or 300 cm high. Each slat is viewed at both ends by an Amperex XP2230 phototube whose base was designed to optimize charge and time resolution over this charge range. The electronic schematic for the TOF array is shown in fig. 13.

The charge calibration of each scintillator is accomplished by selecting a set of fragments whose trajectories have been determined and establishing the relation between charge and the product of the ADC signals from the two tubes on each slat using the function:

Prod(Z) = s*Z**2/(a*Z**2+b*Z+c) * Prod(Z=6).

We use the ADC product to cancel out any simple exponential attenuation effects in the scintillator. We use this form to take account of the saturation properties of the scintillator material. The resulting charge distribution for a single slat is shown in fig. 14.

To determine the mass of a fragment we must calibrate the TOF TDCs. We determine the flight time from the TDC value, start time offset (t0), flight pathlength (L), and time-channel function. To determine t0 we sprayed a constant rigidity beam across all slats. Since we are using leading edge rather than constant fraction discriminators, we must correct the observed TDC channel for pulse height effects. The ADC corrected TDC spectrum for constant R beam particles is shown in fig. 15, showing a resolution of 200ps(FWHM).

To complete the particle identification we obtain mass, m, from the following relation:

$$m = RZ\frac{c}{L}\left((t+t0)^2 - (L/c)^2\right)^{\frac{1}{2}}.$$

The raw rigidity versus slat distribution for charge 1 particles is shown in fig. 16. The mass distribution for charge 1 fragments is shown in fig. 17.

Before going into the results of our experiment we present here some of the plans for Phase II detector systems. In confining our measurements to charged particles we are unable to reconstruct channels having a free neutron in them and we miss all of the energy transferred to the fragments that is dissipated as photons. We would like to augment our facility detector system with a large acceptance neutrals detector and we have borrowed a 28cm x 28cm x 30cm segmented NaI array for testing. A sample output showing hits in 3 adjacent 4cm x 4cm cells is shown in fig. 18.

We expect to use the HISS facility to investigate very high charge and mass fragments from U interactions. In velocity regions of small delta ray production we expect the charge resolution of the TOF scintillators to be greater than 1. To provide the large acceptance needed at HISS we chose to develop a gas based identification system. Consequently we are developing a very large area multiple sampling ionization chamber (MUSIC) detector to give single charge resolution at U. At the Bevalac we work in a region of charge-velocity where the Landau distribution for thin detectors suggests that the charge resolution at constant velocity for a 50mg/cm**2 detector is worse than for 50 measurements from 1mg/cm**2 detectors. An ionization detector responds to energy lost in traversing it, the difference arising from high energy delta rays which exit the detector.

We have tested the chamber shown schematically in fig. 19. The electron cloud around a track drifts downward in the 300V/cm field, through a grounded 95% transmitting Frisch grid and onto 64 anode wires spaced 1 cm apart. The signal from each anode is strobed onto a CCD array being shifted at 10MHz. On receipt of a trigger signal the CCD collection is halted and the array is shifted out to an ADC array at 20kHz, where the computer takes it and places it in the data stream. The electronics, based on the TPC system, are shown in fig. 20.

To complete the HISS Phase II detector arrays we must also increase our acceptance for light fragments. We were limited in the 12C experiment to +/-140Mev/c perpendicular momentum, causing an acceptance for protons of only 50%. Therefore we are adding 40 more TOF slats and building a single gas volume drift chamber 2m x 5m x 1.2m. The Phase II detector array is shown in fig. 21. The cave area showing the Phase I drift chambers, TOF well, and MUSIC detector is shown in fig. 22.

We now present some preliminary results from the 1GeV/nuc 12C experiment. The reaction we have studied can be written schematically as:

$$12C + T \rightarrow (channel) + T'$$

where channel means any final state for the 12 nucleons originally in the C nucleus (e.g. 11B+p or 3 alphas) and T´ is the final state of all target nucleons. The 11B fragments can be formed only in the 11B+p channel but the 4He fragments can be formed in a large number of different channels. In our experiment we attempt to measure complete (i.e. 12 nucleon) channels. After correcting for the acceptance of our system we are thus able to measure the relative probability of forming each separate channel in the interaction. We then form the invarient mass for each interaction chánnel and subtract from the mass of the 12C parent to determine the amount of energy transferred to the fragment channel in each interaction. By analysing many fragments from a single interaction we can also take subgroups of fragments and calculate invarient masses for these subgroups to look for preferred intermediate states (e.g. 2 alphas from an 8Be).

The experimental layout is shown in fig. 23 including beam definition devices, large gap superconducting dipole, fragment trajectory drift chambers, and time-of-flight (TOF) scintillator array. The event trigger required a single 12C hit on the target and no 12C signature at DS, indicating that the projectile had been scattered or destroyed.

The first results from our experiment are shown in fig. 24 where we have used all channels having $\Sigma Zf = 6$ and $\Sigma Af = 12$ giving a global excitation energy spectrum. The prominant peak near 30 MeV excitation leads to fragments having 50-200 MeV/c momentum in the projectile rest frame, fragments primarily responsible for observed single particle inclusive momentum distributions. Data out to 400 MeV excitation are from interactions in which large energies are transferred to the 12C system, the energy then being shared among a few multi-nucleon fragments. Energies of 300 MeV shared among 3 alpha particles have been seen suggesting a collective mode transfer of energy such as would be expected from a phonon like exchange mechanism.

In conclusion I would like to say that we have observed the excitation spectrum for fully reconstructed events and seen energies up to 400 MeV transferred to bound fragment systems. We have data for all charged particle channels and for invarient mass calculations for arbitraty particle groupings. Finally, the Phase II detector system should be available at HISS by spring 1983.

This work was supported by the Director, Office of Energy Research, Division of Nuclear Physics of the Office of High Energy and Nuclear Physics of the U.S. Department of Energy under Contract DE-AC03-76SF00098 and National Aeronautics and Space Administration grant number NGR 03-003-513.

# SINGLE PARTICLE INCLUSIVE HAS SHOWN US:

PERSISTENCE OF VELOCITY → MAGNETIC SPECTROMETERS BECOME $\frac{Z}{M}$ SPECTROMETERS

FACTORIZATION (TARGET INDEPENDENCE) → TARGET AND PROJECTILE FRAME PHYSICS IS EQUIVALENT

# PROBLEMS ARE:

ALL SPECTRA LOOK LIKE PHASE SPACE (THERMAL MODEL)

WE NEED BETTER DEFINITION OF THE FINAL STATE IN ORDER TO AVOID INTEGRATION OVER THE UNSEEN PRODUCTS.

Fig. 1

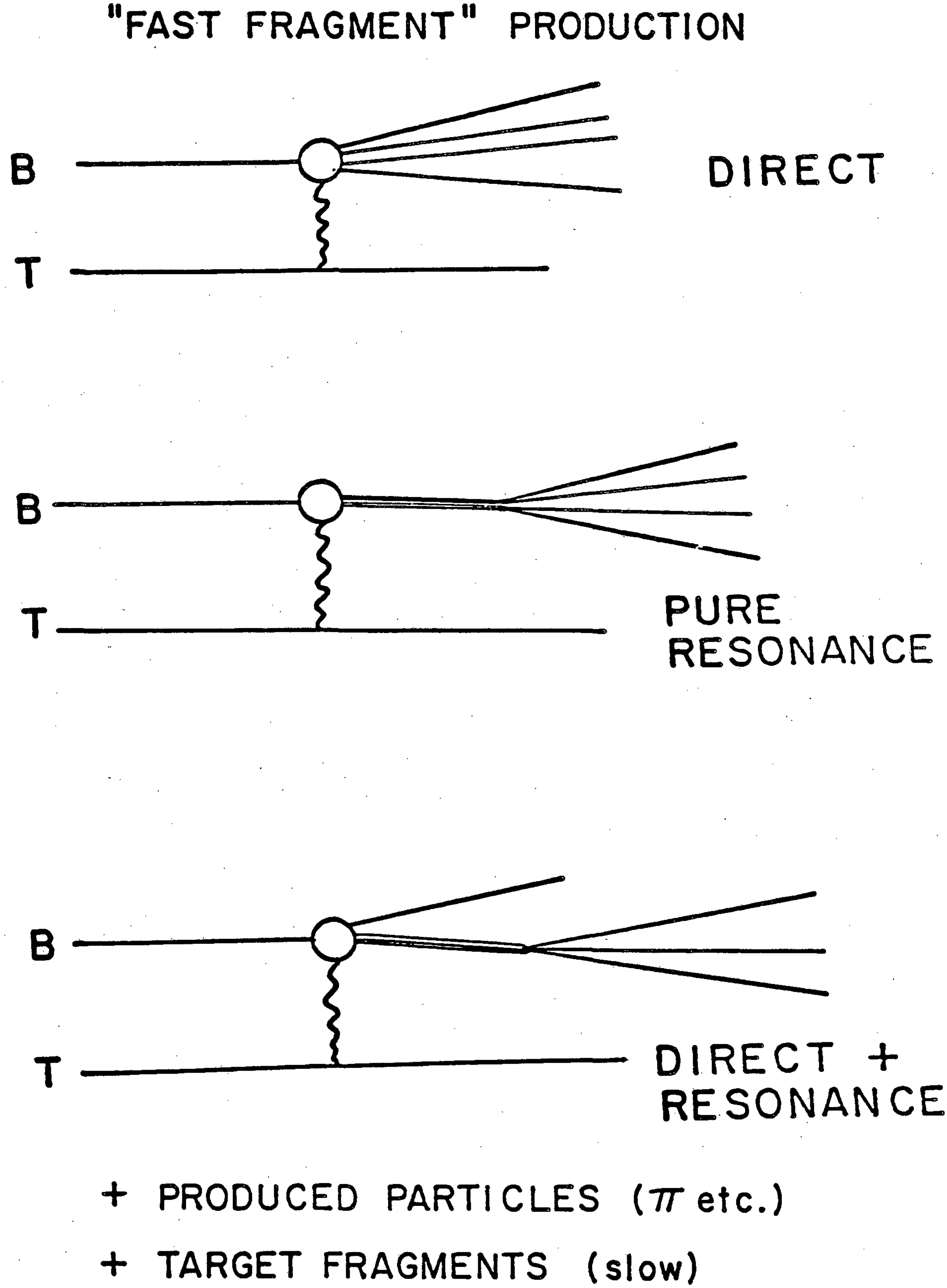
"FAST FRAGMENT" PRODUCTION
B
T
DIRECT
B
T
PURE
RESONANCE
B
T
DIRECT +
RESONANCE
+ PRODUCED PARTICLES (π etc.)
+ TARGET FRAGMENTS (slow)

Fig. 2

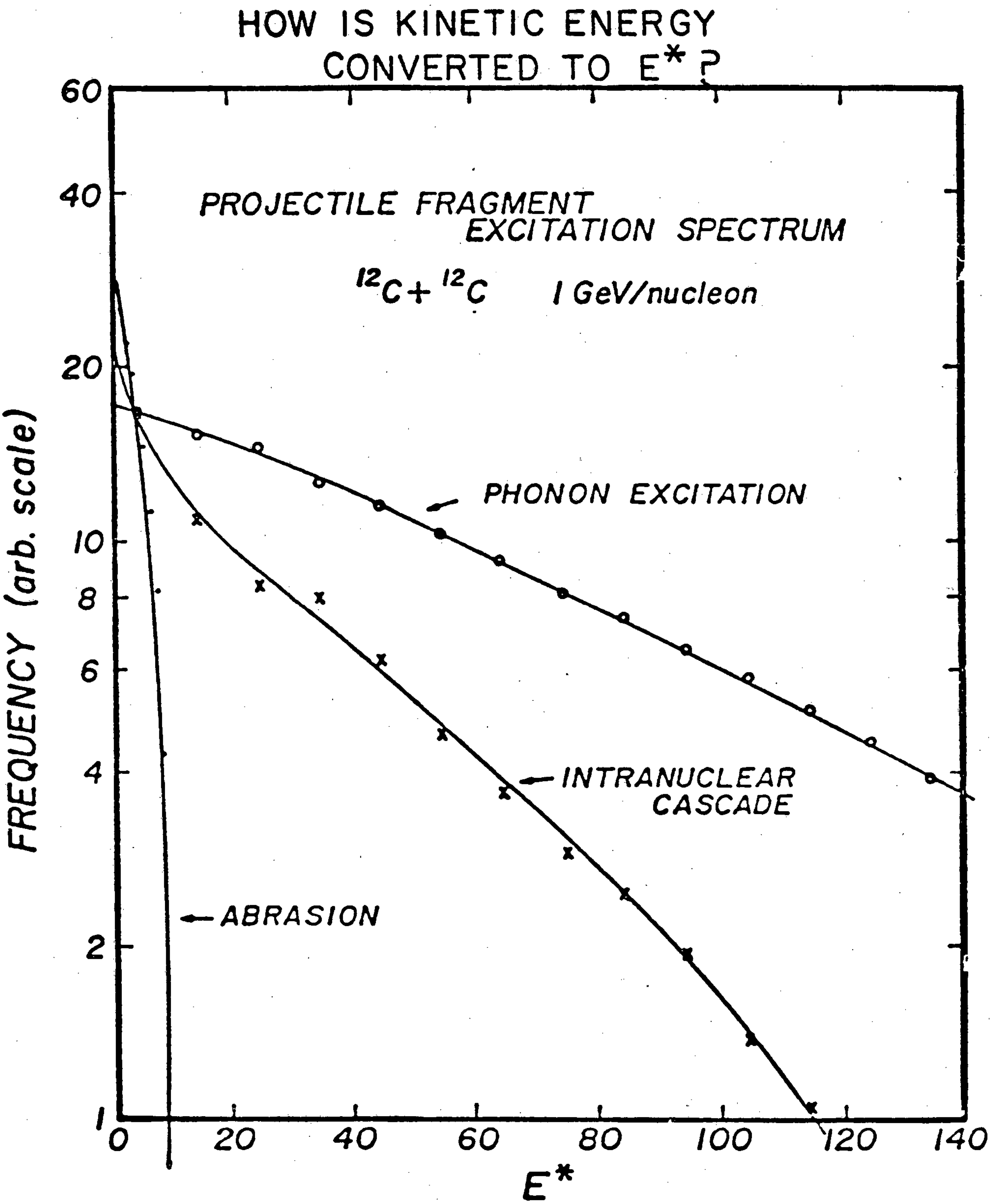
HOW IS KINETIC ENERGY
CONVERTED TO E* ?
PROJECTILE FRAGMENT
EXCITATION SPECTRUM
12C + 12C
1 GeV/nucleon
PHONON EXCITATION
INTRANUCLEAR
CASCADE
ABRASION
FREQUENCY (arb. scale)
E*
60
40
20
10
8
6
4
2
1
0
20
40
60
80
100
120
140

Fig. 3

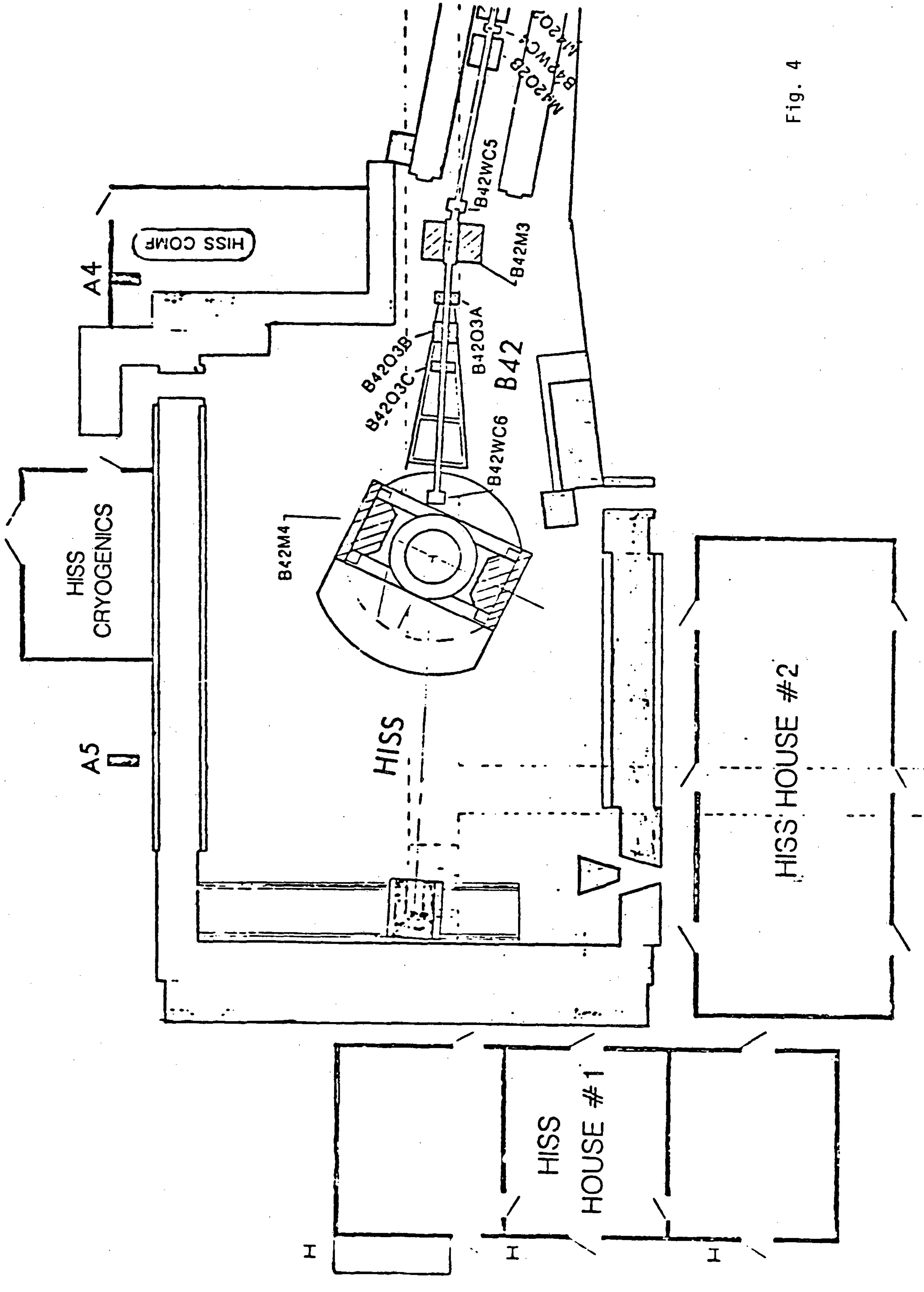
HISS CRYOGENICS
HISS COMP
A4
A5
HISS
B42
B42M3
B42M4
B42WC5
B42WC6
B42O3A
B42O3B
B42O3C
M42O2B
HISS HOUSE #1
HISS HOUSE #2

Fig. 4

## HEAVY ION SPECTROMETER SYSTEM GROUP

| | |
|---|---|
| E. BELEAL | LBL |
| F. BIESER | LBL |
| M. BRONSON | LBL |
| H. CRAWFORD | UC-SSL |
| J. ENGELAGE | LSU |
| I. FLORES | UC-SSL |
| D. GREINER | LBL |
| M. JOHNSON | UC DAVIS |
| P. LINDSTROM | LBL |
| C. McPARLAND | UC-SSL |
| J. PORTER | LBL |
| D. OLSON | LLNL |
| H. SANN | GSI |
| R. WADA | LBL |

Fig. 5

# HISS PHASE I EXPERIMENTS

COULOMB DISSOCIATION OF $^{16,18}O$--LLL, SSL, LBL

GOALS: EXCITATION OF GIANT RESONANCES IN $^{16,18}O$ DECAY

INVARIANT MASS SPECTRA FROM $^{12}C$--LSU, SSL, UCD, NRL, LBL

GOALS: EXCITATION SPECTRA FROM EXCLUSIVE MODES
SEARCH FOR STRUCTURE IN INVARIANT MASS SPECTRA

FRAGMENTATION OF $^{56}FE$--SSL, NRL, LBL

GOALS: SEARCH FOR COLLECTIVE EFFECTS EVIDENCED BY STRUCTURE IN INVARIANT MASS SPECTRA

MEASUREMENTS OF LARGE $P_T$ FRAGMENTS--INS, LBL

GOALS: STUDY COLLECTIVE EFFECTS NEAR KINEMATIC LIMIT AND THE ASSOCIATED MULTIPLICITIES

TWO PARTICLE CORRELATIONS AT SMALL $\Delta P$--UCLA, UCD, LBL

GOALS: USE SECOND ORDER INTERFERENCE BETWEEN IDENTICAL PARTICLES TO DETERMINE INTERACTION VOLUME AND TIME

Fig. 6

PHASE I DETECTOR ARRAY

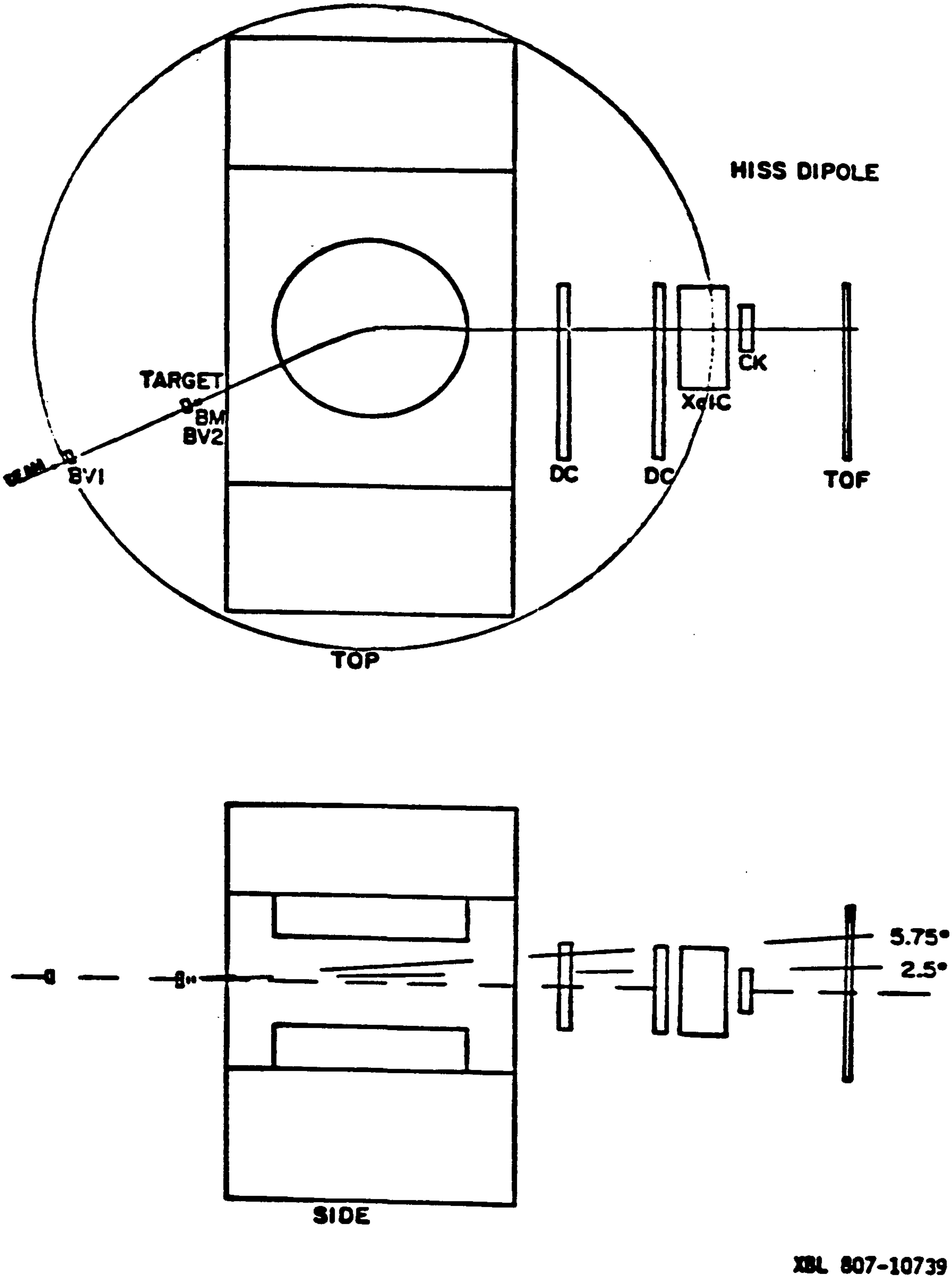


Fig. 7

## LAYOUT OF THE EXPERIMENTAL SETUP FOR E512

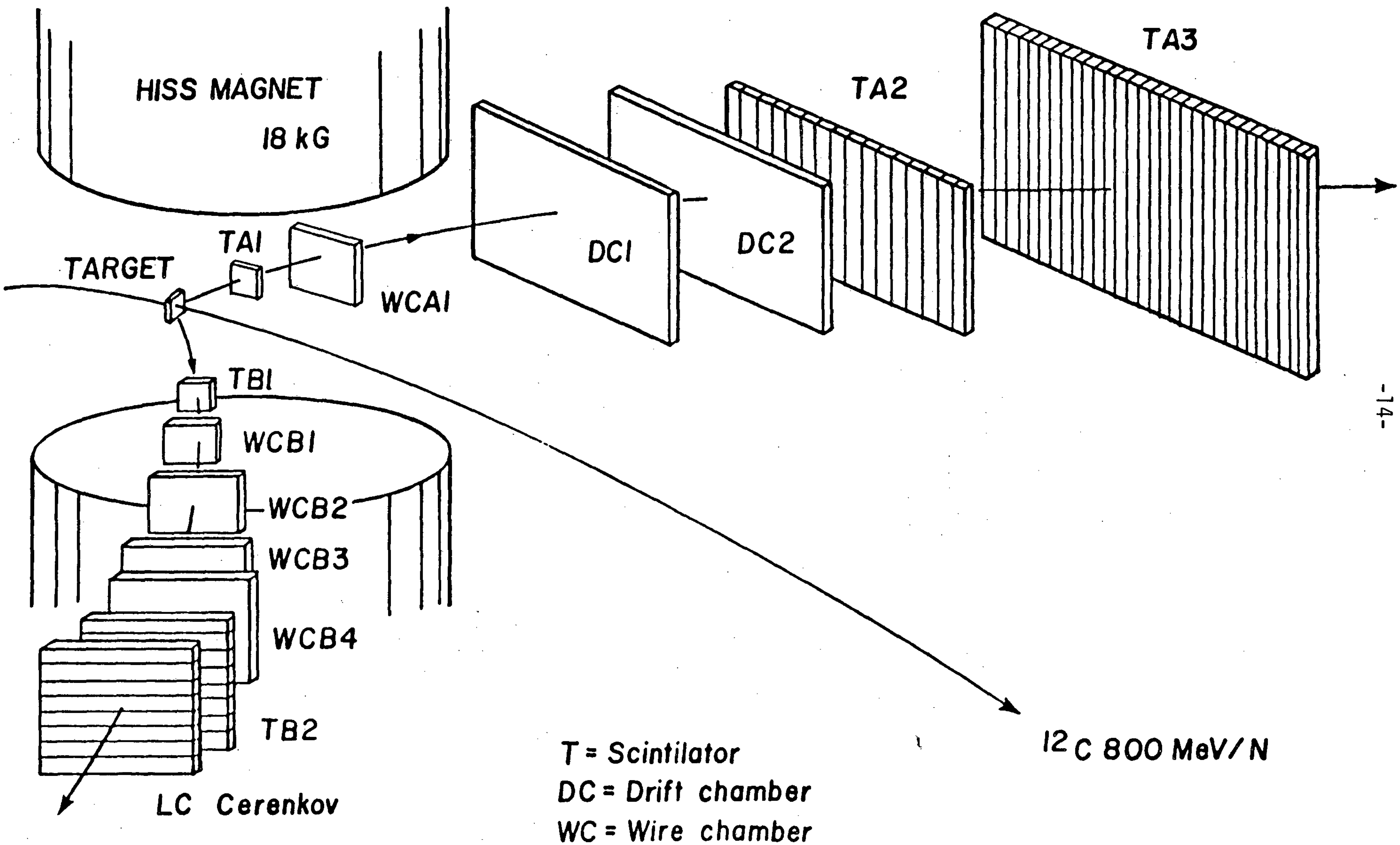


Fig. 8

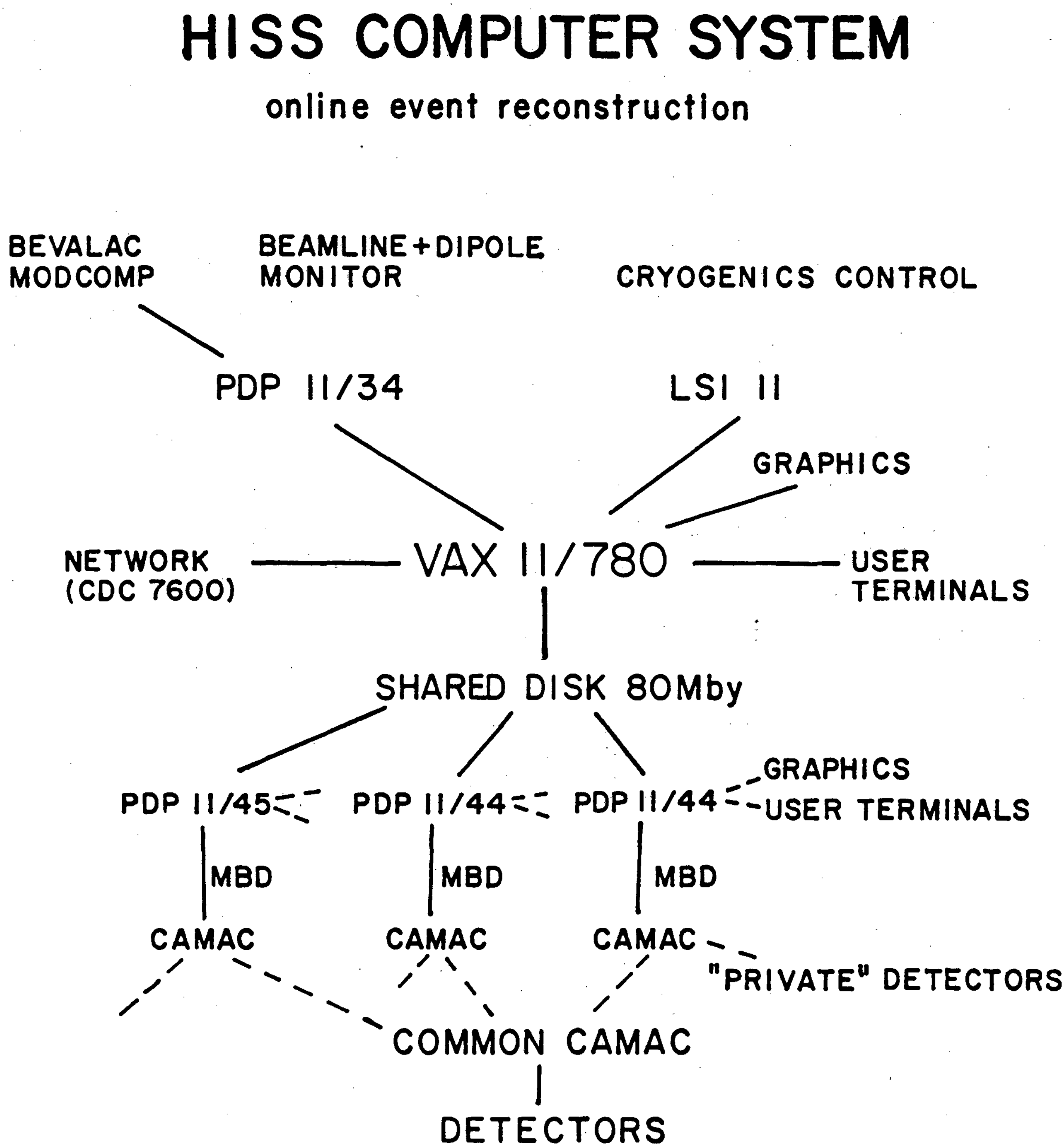
HISS COMPUTER SYSTEM
online event reconstruction
BEVALAC MODCOMP
BEAMLINE + DIPOLE MONITOR
CRYOGENICS CONTROL
PDP 11/34
LSI 11
GRAPHICS
NETWORK (CDC 7600)
VAX 11/780
USER TERMINALS
SHARED DISK 80Mby
PDP 11/45
PDP 11/44
PDP 11/44
GRAPHICS
USER TERMINALS
MBD
MBD
MBD
CAMAC
CAMAC
CAMAC
"PRIVATE" DETECTORS
COMMON CAMAC
DETECTORS

Fig. 9

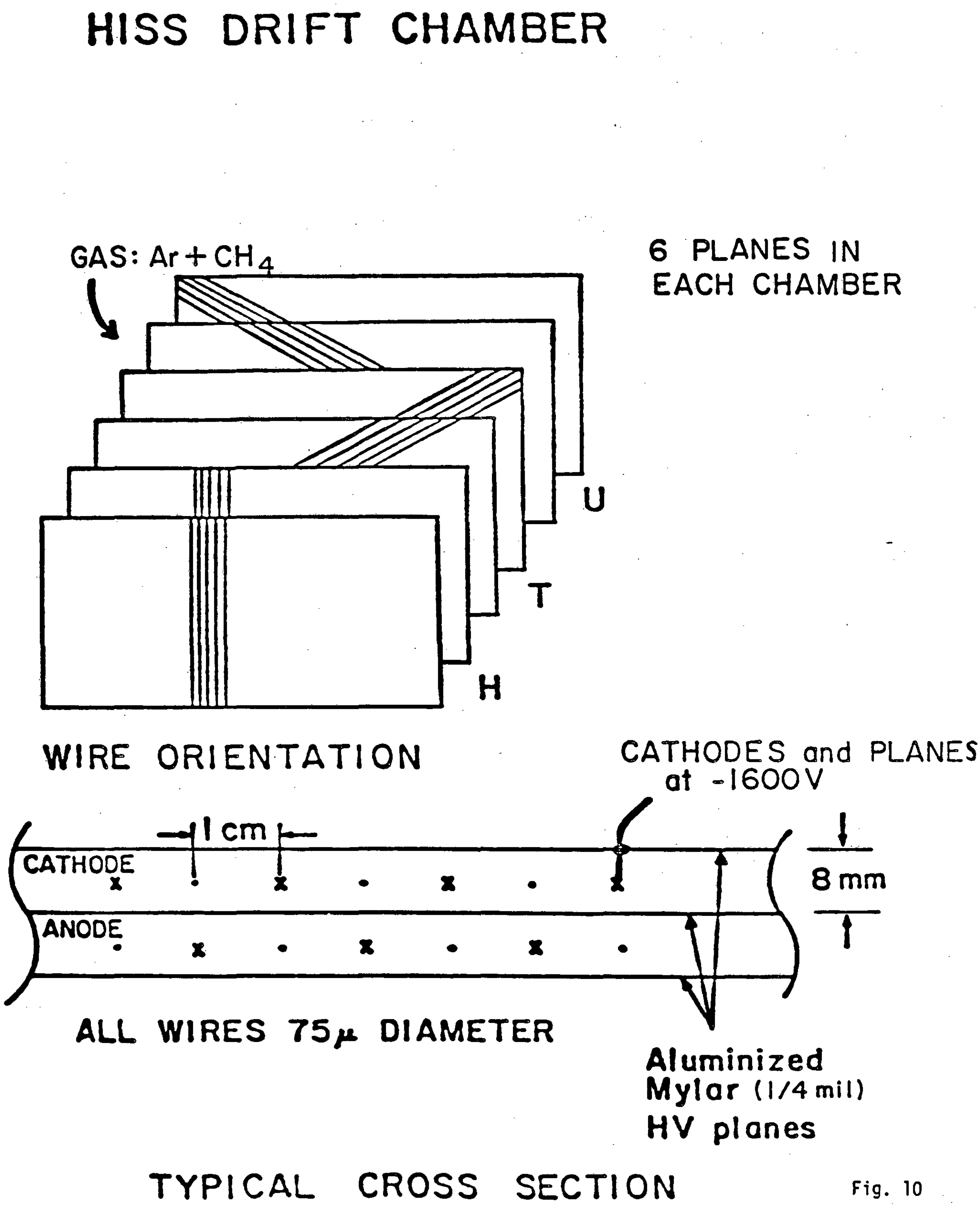
HISS DRIFT CHAMBER
GAS: Ar + CH4
6 PLANES IN
EACH CHAMBER
U
T
H
WIRE ORIENTATION
CATHODES and PLANES
at -1600V
1 cm
CATHODE
ANODE
8 mm
ALL WIRES 75μ DIAMETER
Aluminized
Mylar (1/4 mil)
HV planes
TYPICAL CROSS SECTION

Fig. 10

# HEAVY ION DRIFT CHAMBER FRONT END

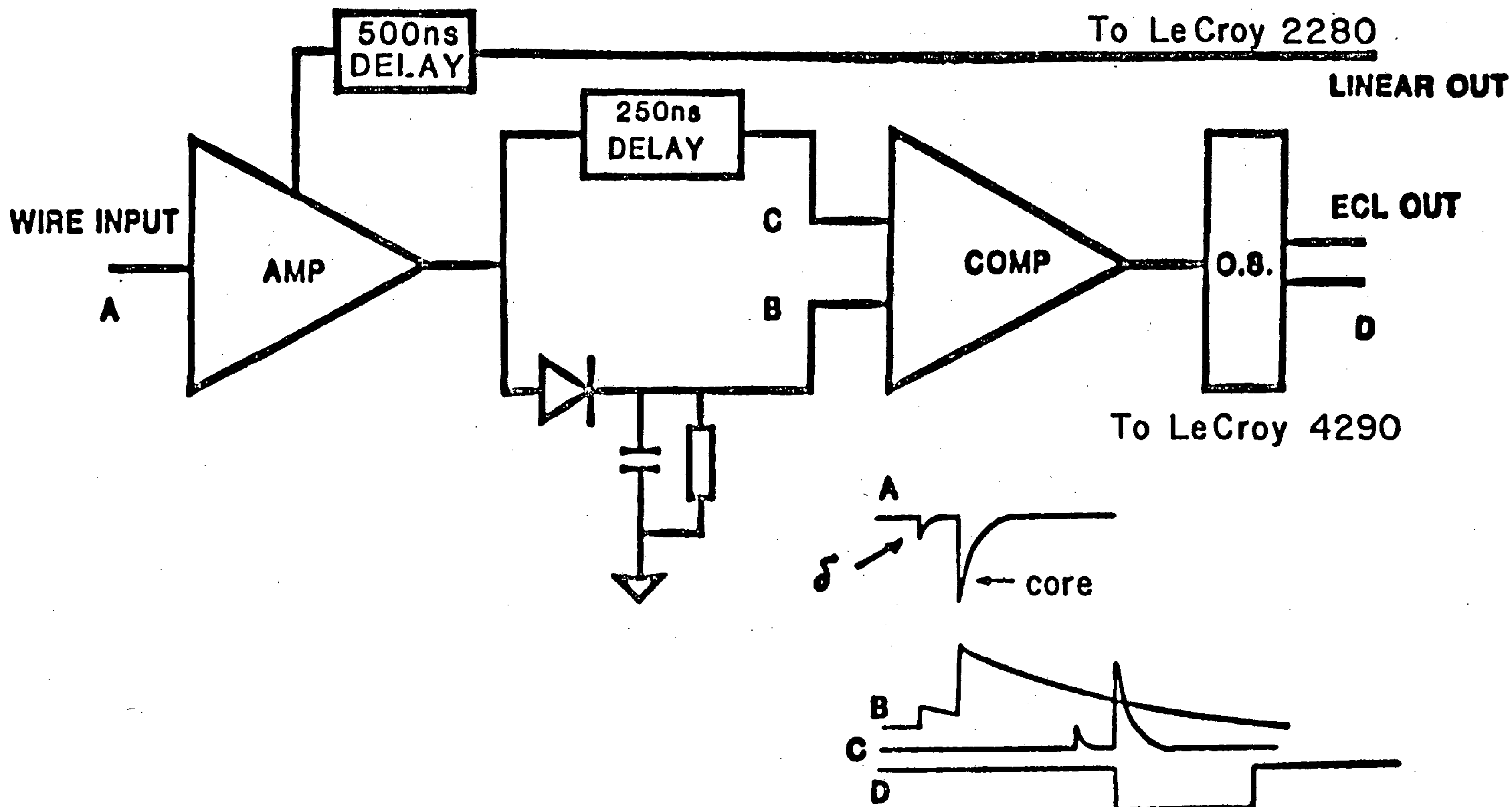


Fig. 11

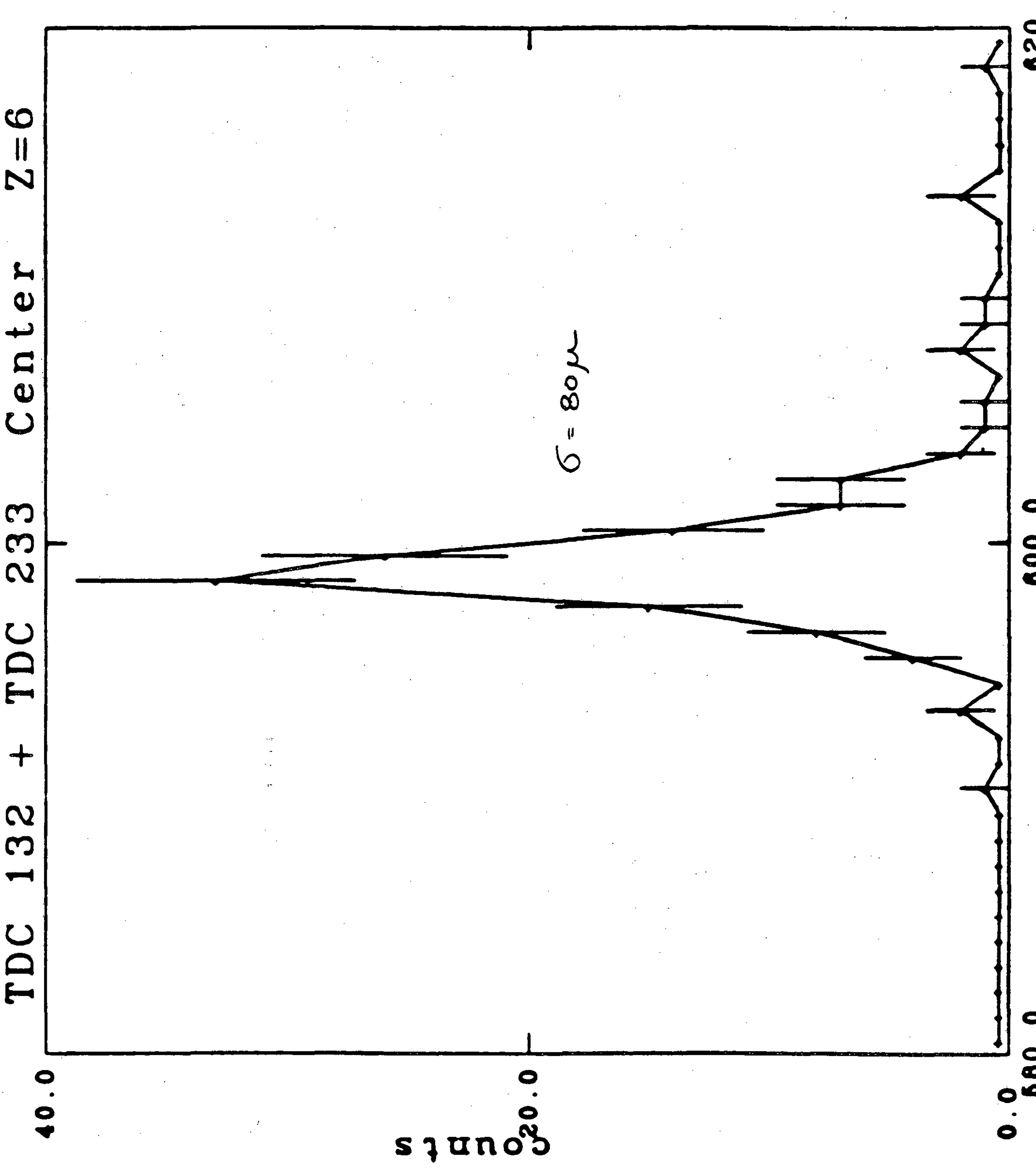
TDC 132 + TDC 233 Center Z=6
σ = 80μ
40.0
20.0
0.0
Counts
580.0
600.0
620.0
TDC SUM

Fig. 12

# TOF ELECTRONICS

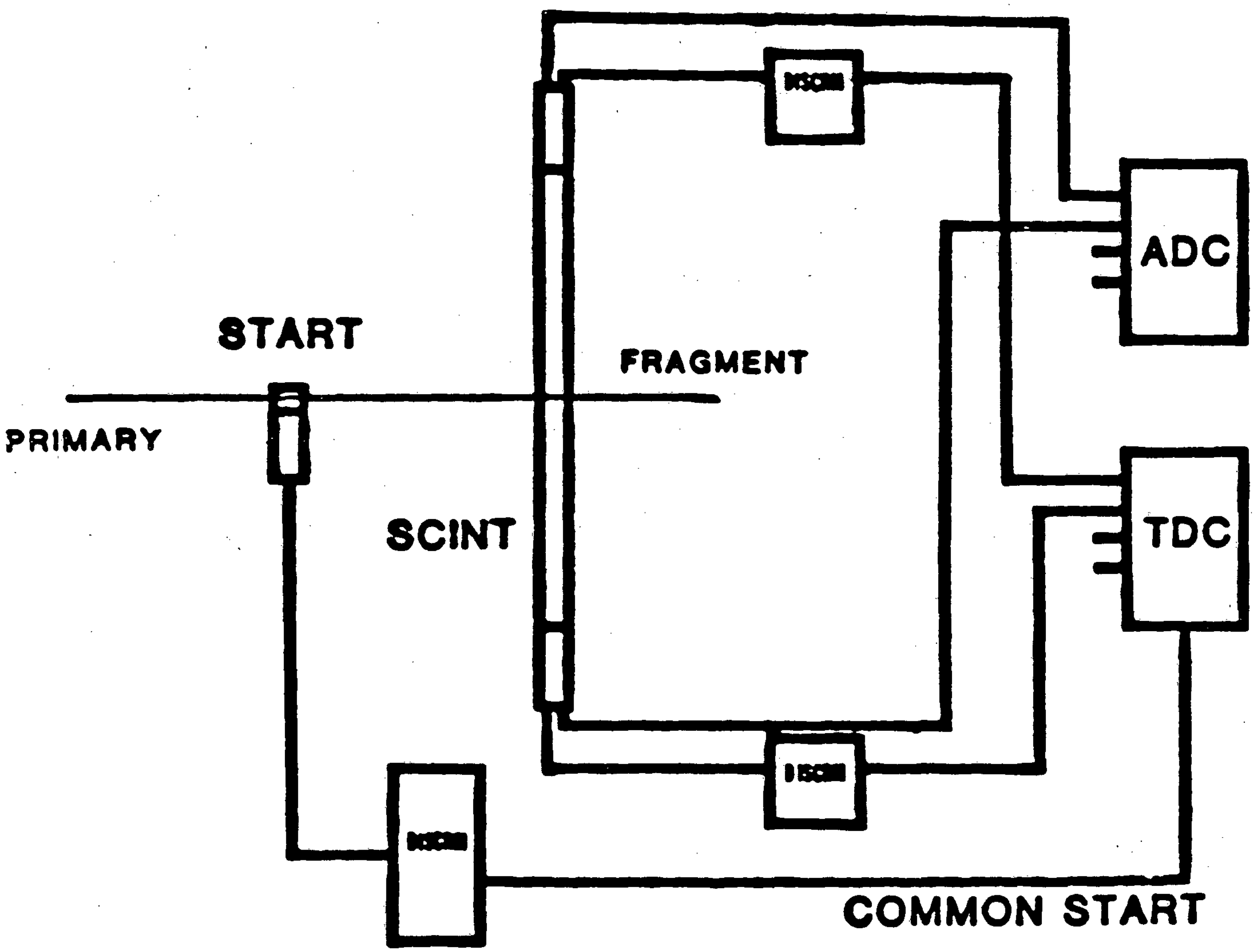


LE CROY 2280 ADC SYSTEM
LE CROY 2228A TDCS
LE CROY 6200 DISCRIMINATORS

Fig. 13

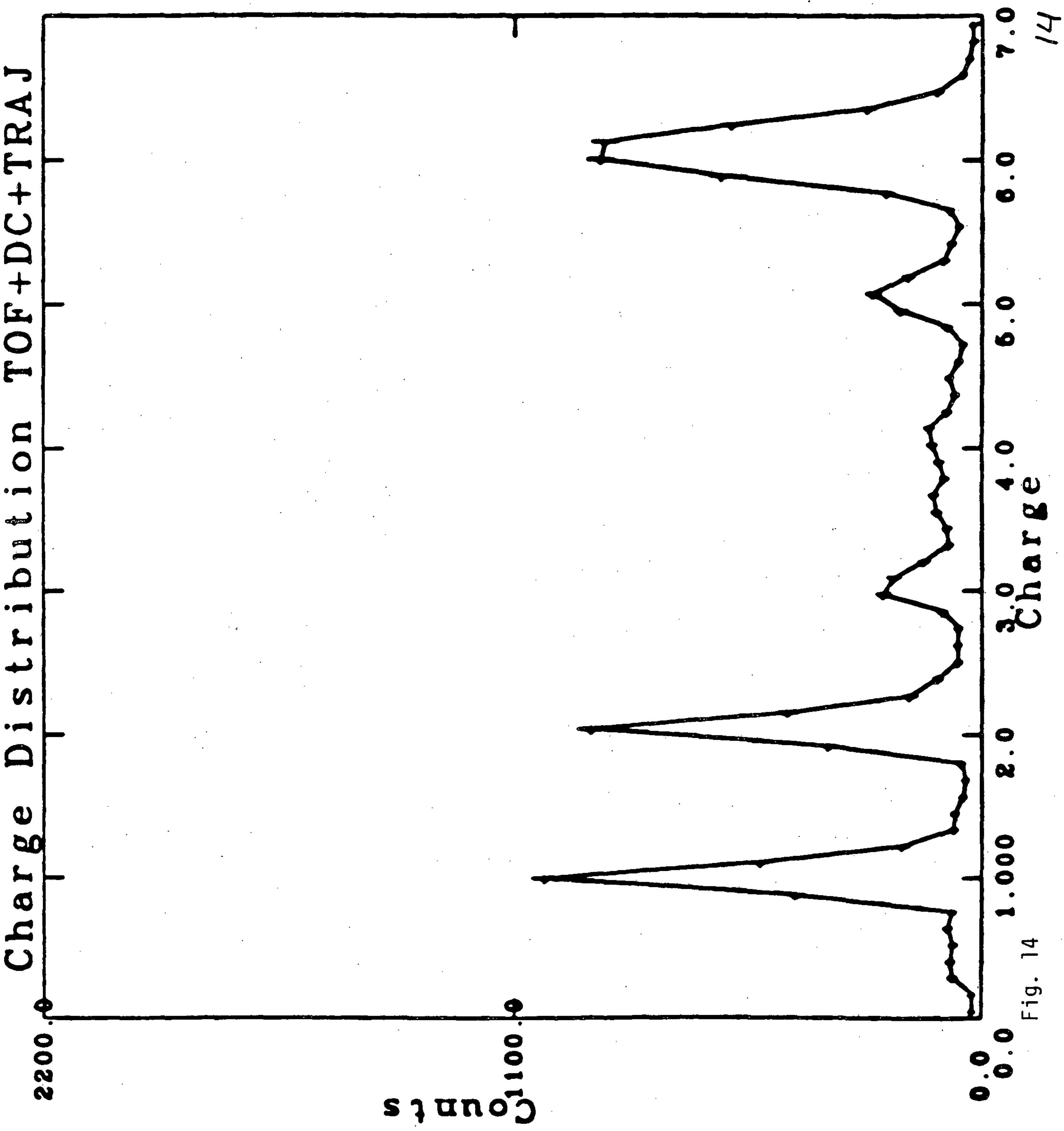
Charge Distribution TOF+DC+TRAJ
Counts
2200.
1100.
0.0
0.0
1.000
2.0
3.0
4.0
5.0
6.0
7.0
Charge
14

Fig. 14

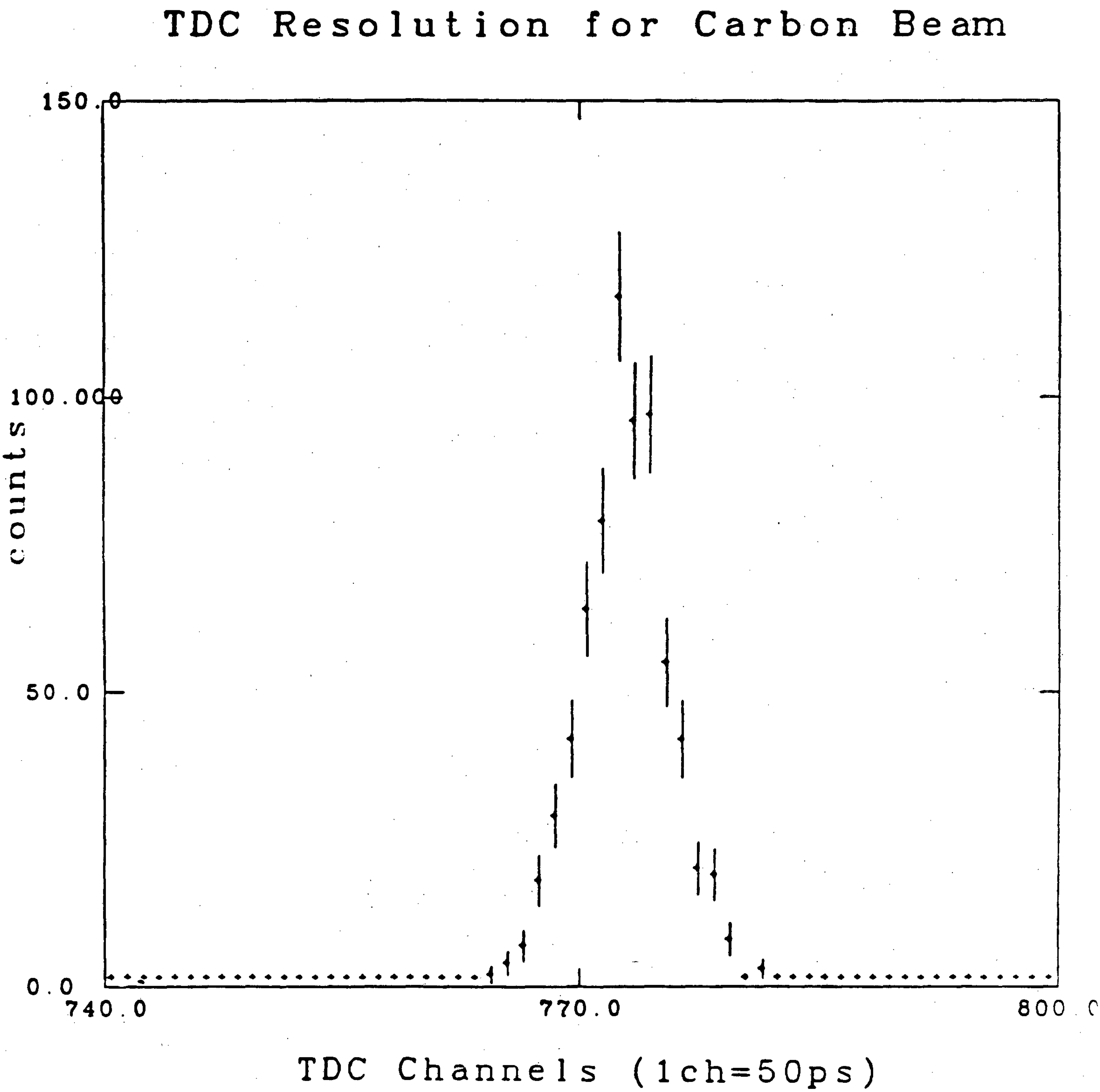
TDC Resolution for Carbon Beam
150.0
100.000
50.0
0.0
counts
740.0
770.0
800.0
TDC Channels (1ch=50ps)

Fig. 15

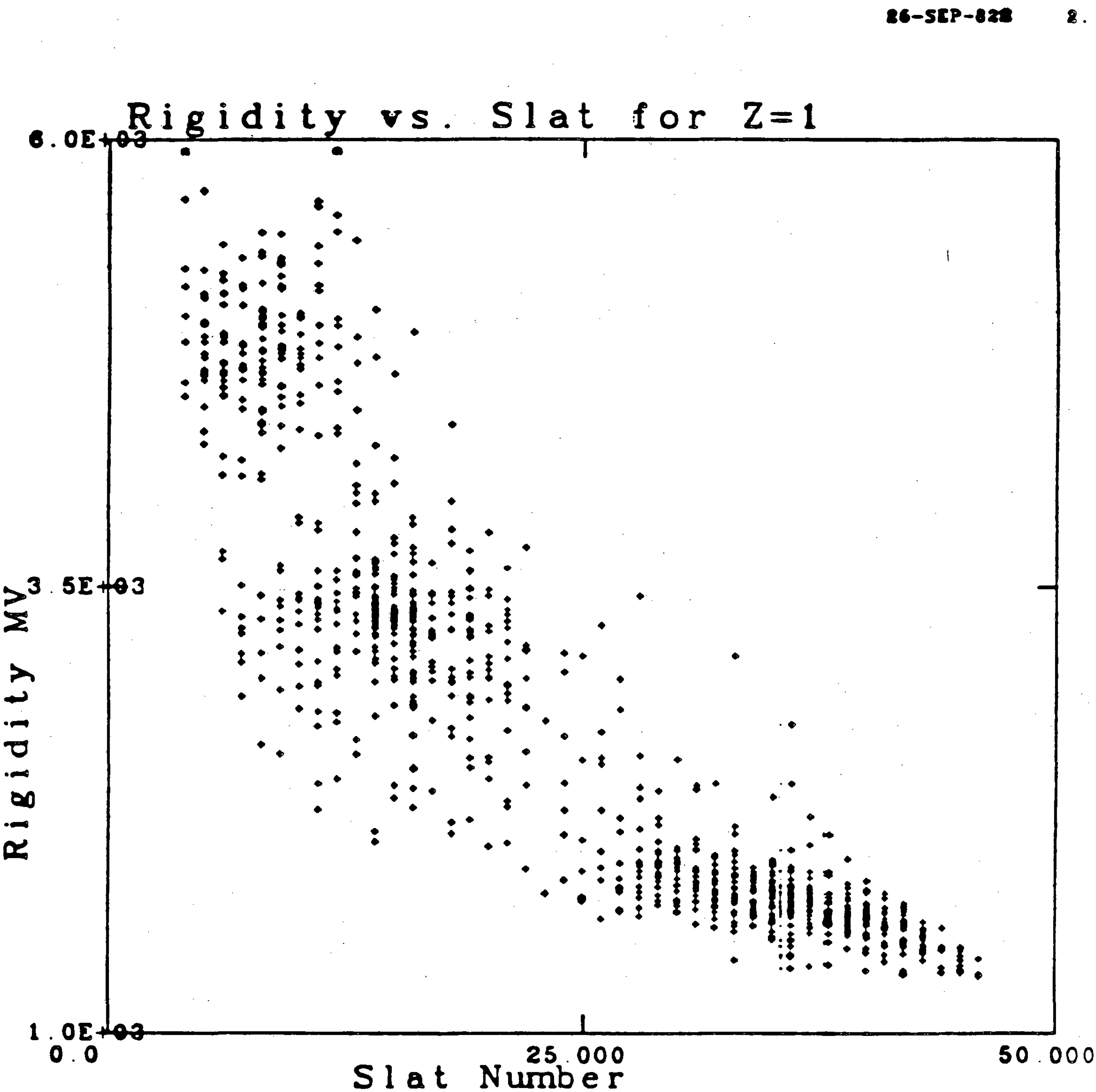
26-SEP-82
2.
Rigidity vs. Slat for Z=1
6.0E+03
3.5E+03
1.0E+03
Rigidity MV
0.0
25.000
50.000
Slat Number

Fig. 16

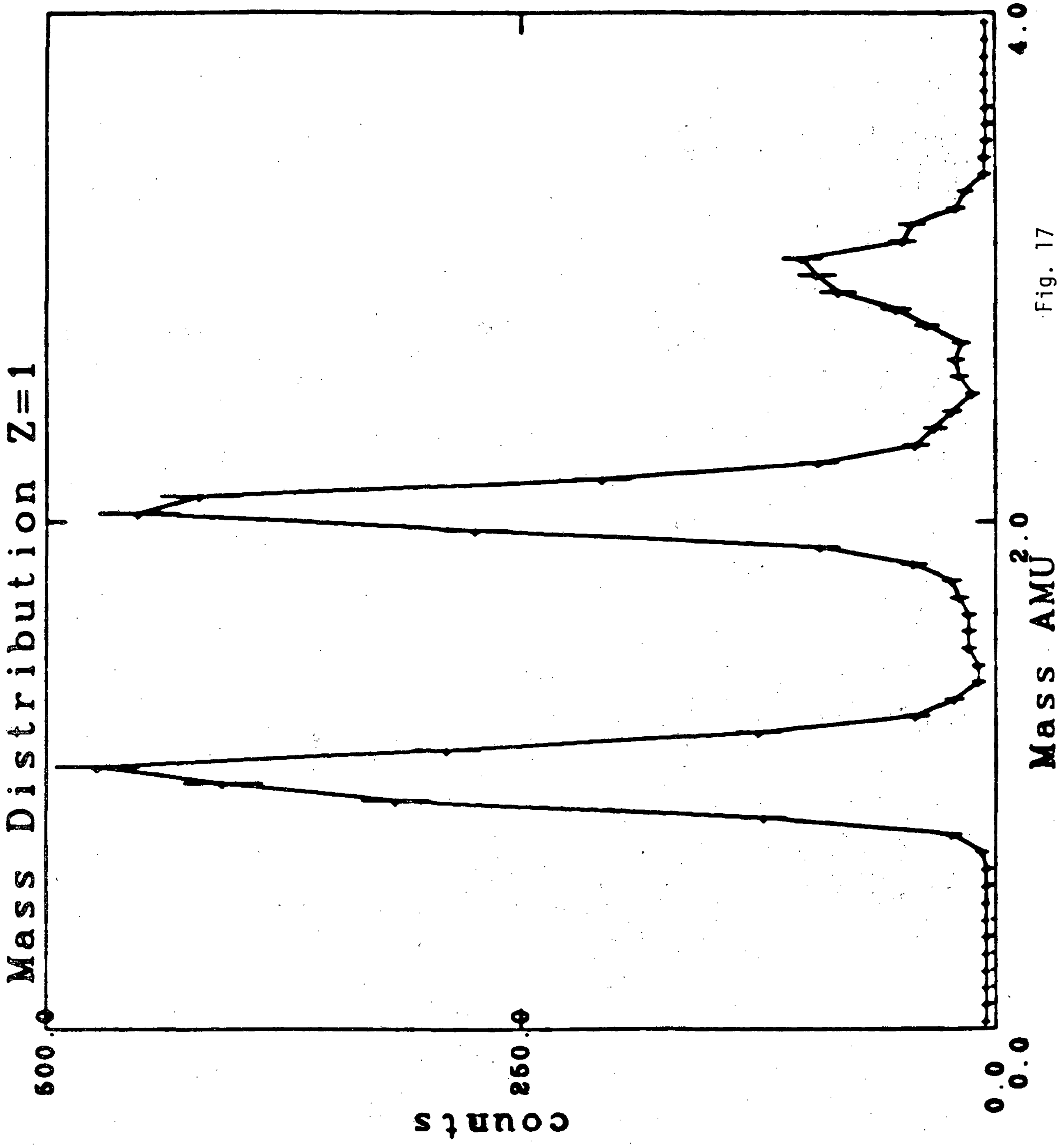


Fig. 17

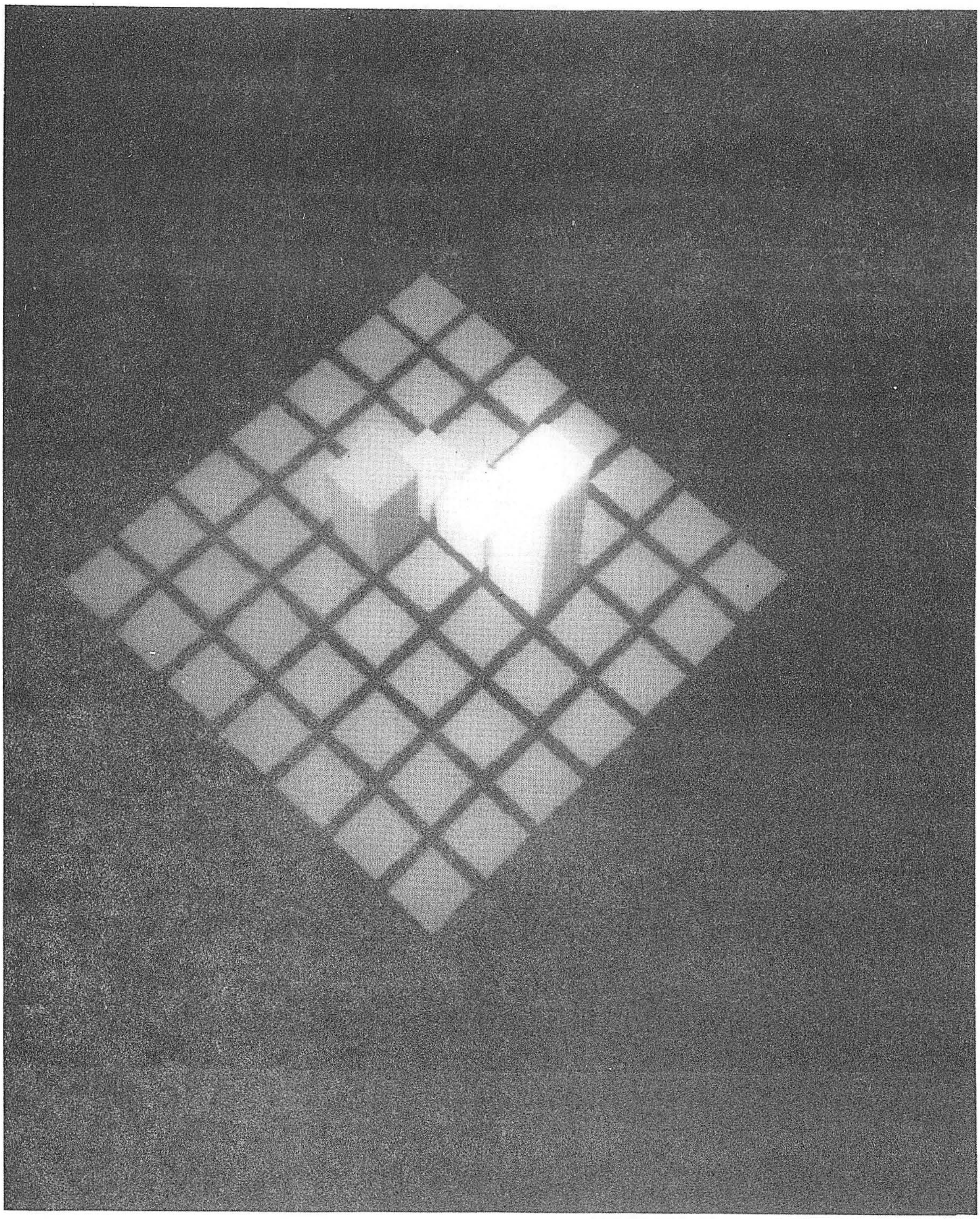

Fig. 18

CBB 828-6823

To measure Z for $6 \leq Z \leq 92$

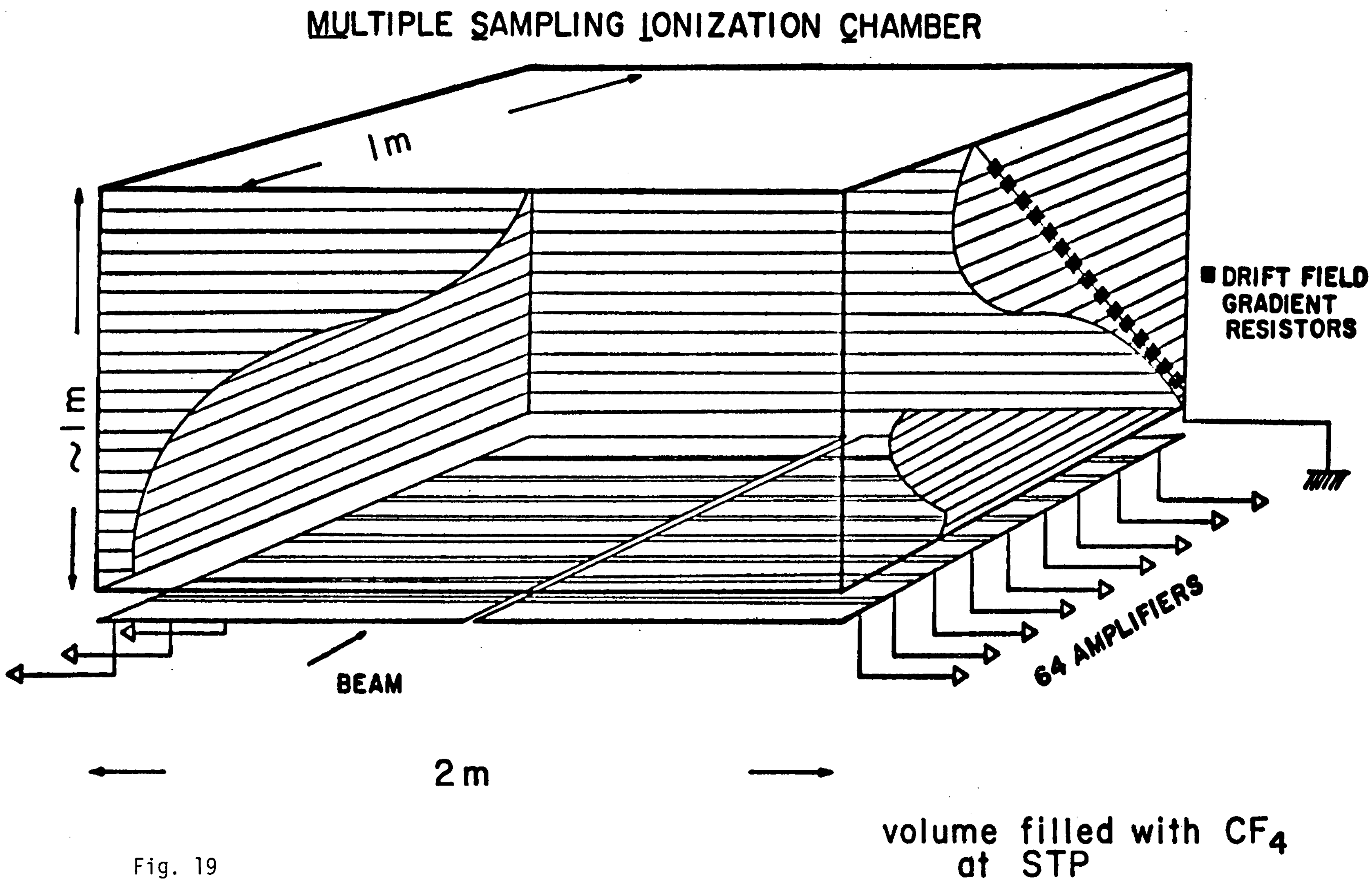


Fig. 19

23 July 80

XeIC ELECTRONICS

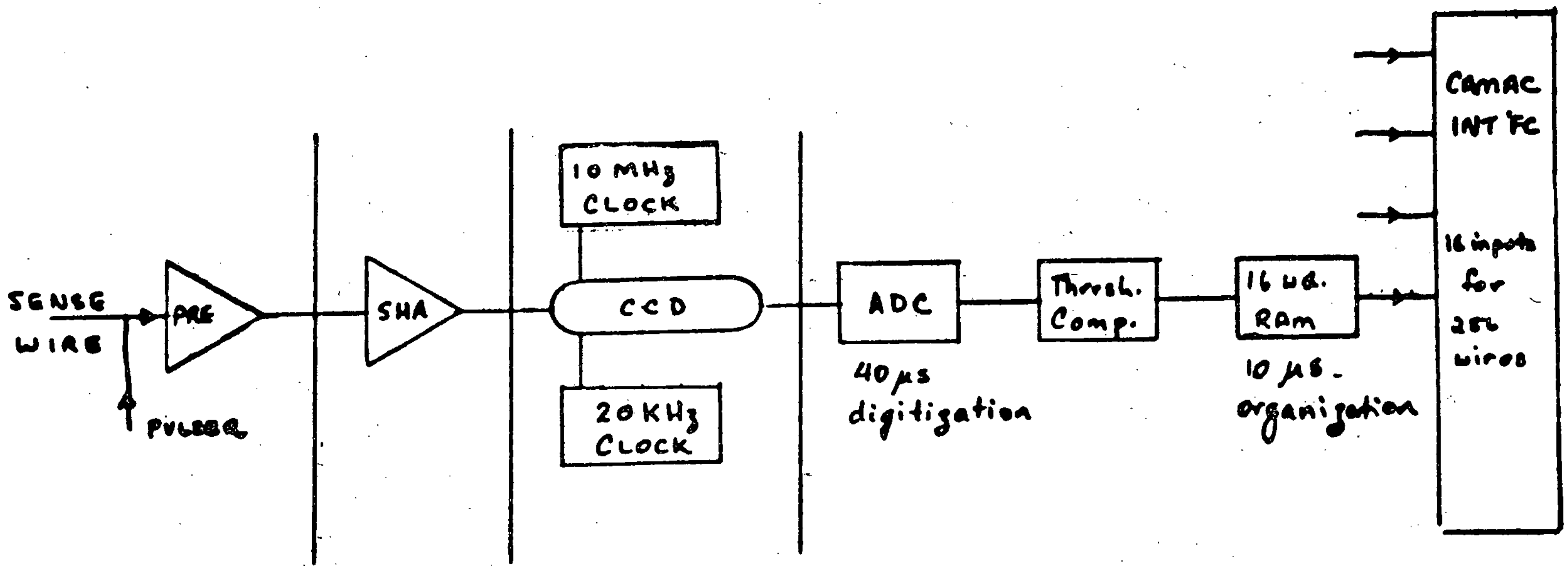


16 CHANNELS / BOARD

EACH BOARD HAS 16-(32bit) WORD RAM
RAM IS FILLED WITH ANY ADC WORDS
GREATER THAN DIGITAL THRESHOLD

RAM'S READ ONTO DATAWAY AT 5MHz (200nsec/WORD)

Fig. 20

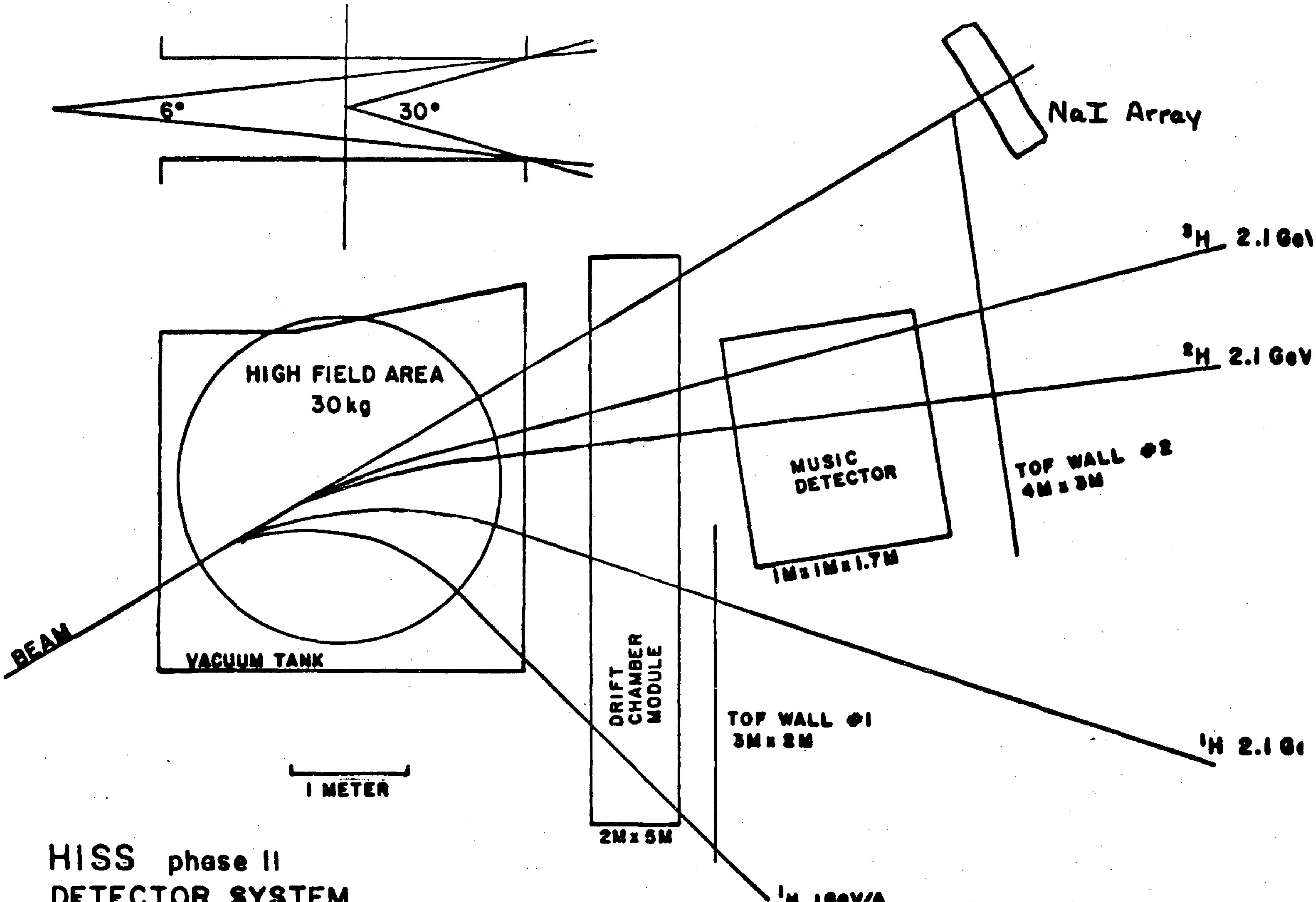


HISS phase II
DETECTOR SYSTEM

Fig. 21

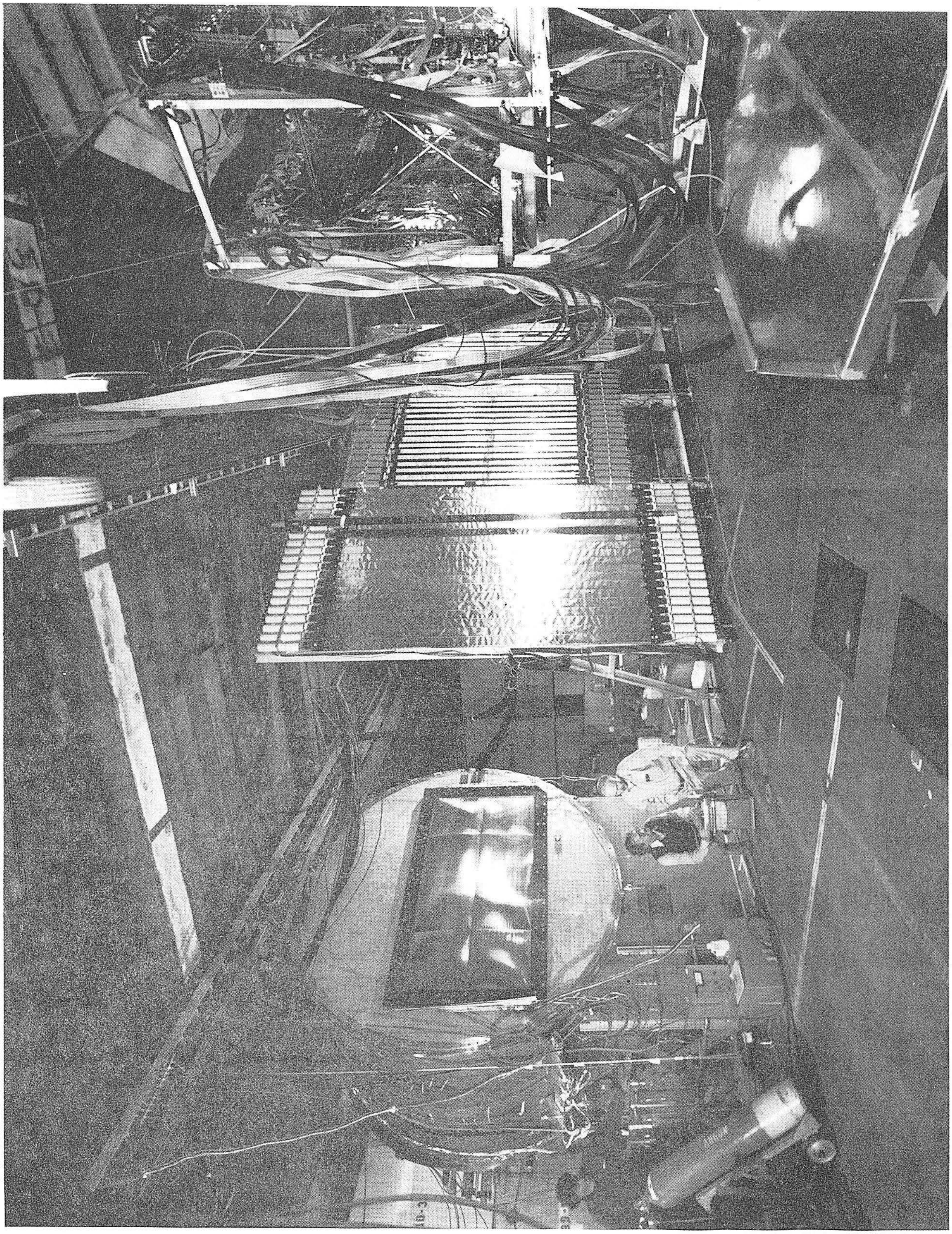

CBB 828-7538

Fig. 22

# MULTI-PARTICLE FINAL STATES FROM $^{12}C$ at 1 GeV/n

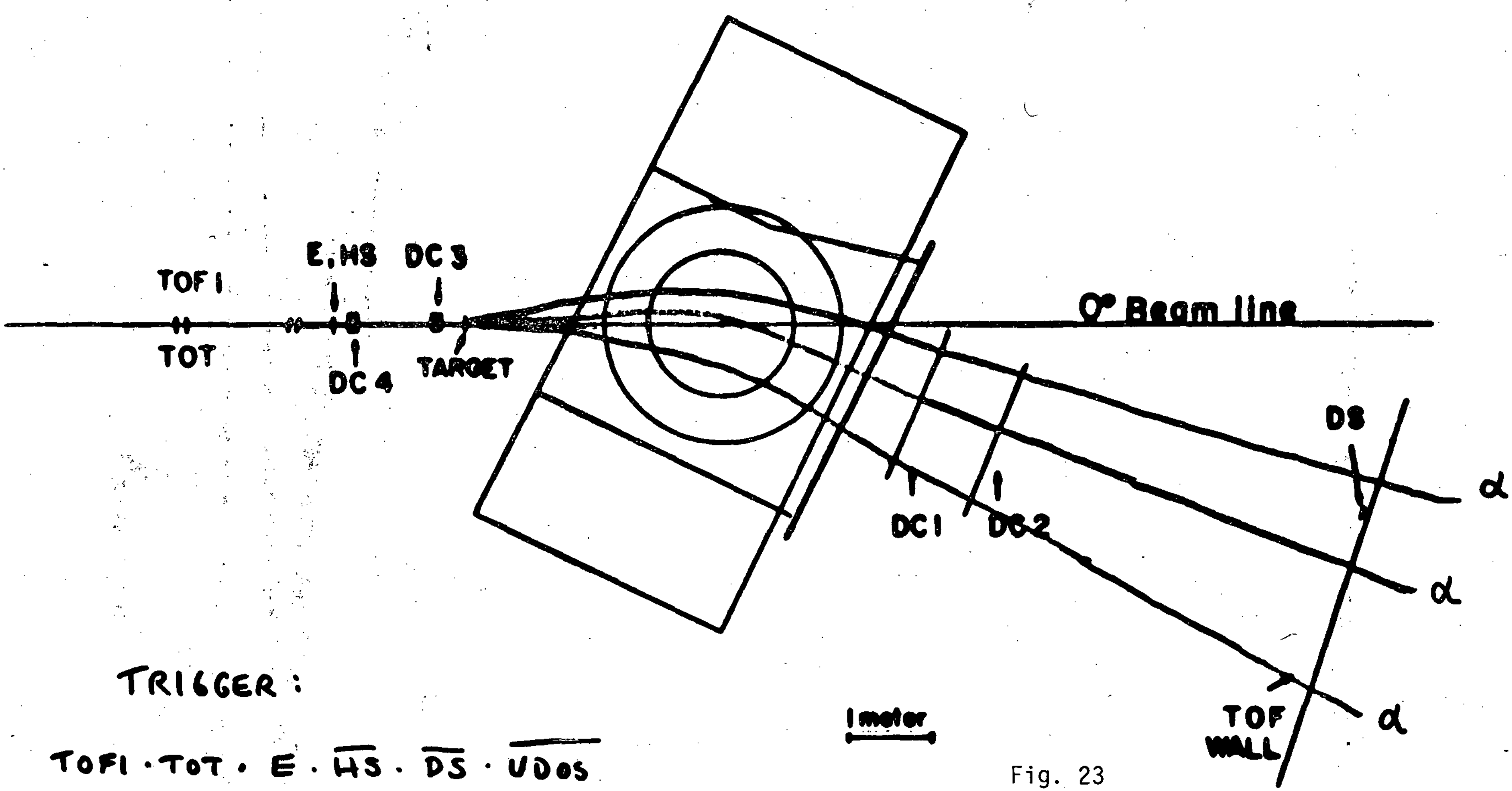


Fig. 23

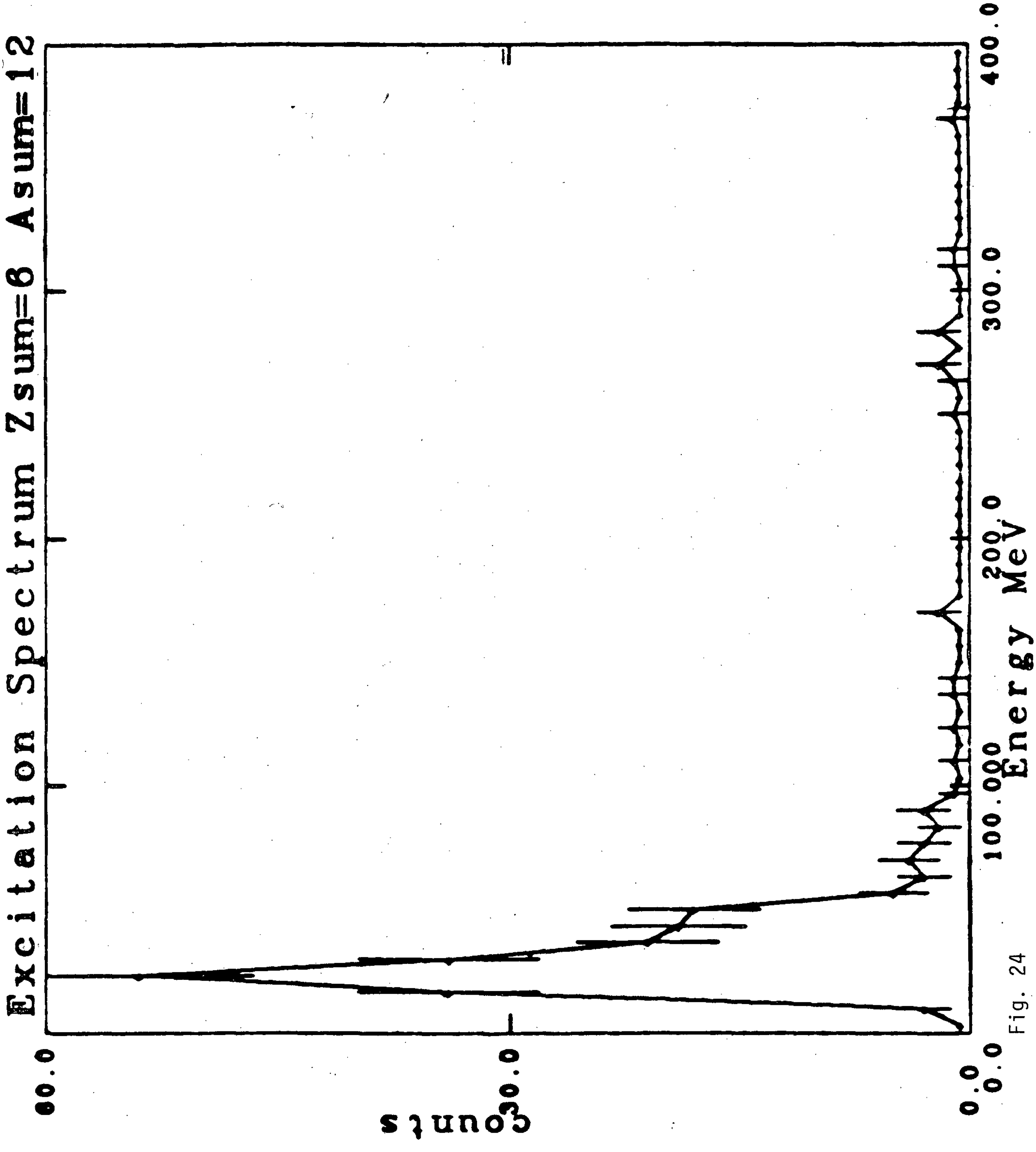

Excitation Spectrum Zsum=6 Asum=12
Counts
60.0
30.0
0.0
0.0
100.0
200.0
300.0
400.0
Energy MeV


Fig. 24

*TECHNICAL INFORMATION DEPARTMENT*
*LAWRENCE BERKELEY LABORATORY*
*UNIVERSITY OF CALIFORNIA*
*BERKELEY, CALIFORNIA 94720*